Available online at www.sciencedirect.com
ScienceDirect
Journal of Catalysis 249 (2007) 52–58
JOURNAL OF CATALYSIS
www.elsevier.com/locate/jcat

Spectroscopic characterization of iron nanoparticles in Fe-mesoporous silicate catalysts

K. Bachari [a], J.M.M. Millet [b,*], P. Bonville [c], O. Cherifi [a], F. Figueras [b]

[a] *Laboratoire de Chimie du Gaz Naturel, Faculté de Chimie, BP 32, 16111, El Alia, U.S.T.H.B., Bab Ezzouar, Algérie*
[b] *Institut de Recherches sur la Catalyse et l'Environnement de Lyon, CNRS, Université Claude Bernard Lyon I, UMR5256, 2 avenue Albert Einstein, Villeurbanne, F-69626 Cedex, France*
[c] *CEA, Centre d'Etudes de Saclay, DSM/DRECAM/Service de Physique de l'Etat Condensé, F-91191 Gif-sur Yvette Cedex, France*

Received 4 January 2007; revised 23 March 2007; accepted 25 March 2007
Available online 21 May 2007

Abstract

Iron-containing mesoporous silicates used as catalysts for the alkylation of benzene with benzyl chloride were characterized using several spectroscopic techniques. Electron spin resonance and Mössbauer spectroscopies, along with electron microscopy and X-ray diffraction, allowed differentiation of several iron species. These species correspond to (i) hematite (α-Fe_2O_3) particles, (ii) very small "isolated" or oligomeric Fe^{III} species possibly incorporated in the mesoporous silica wall, and (iii) Fe^{III} oxide clusters either isolated or agglomerated, forming "rafts" at the surface of the silica and exhibiting ferromagnetic ordering. Because of their agglomeration, these clusters appear with a two-peak size distribution, with one peak (ca. 2–3 nm diameter) corresponding to the isolated clusters formed in the mesopores and still embedded in them and the other (ca. 10 nm) corresponding to the agglomerates spread on the surface of the mesoporous silica particles. These species, which should be the most active species, appear similar to those recently observed at the surface of tunsgtated zirconia with iron promoter.

Keywords: Mesoporous oxide; Nanosized iron oxide; Benzene benzylation; Friedel–Crafts alkylation; Mössbauer and ESR spectroscopy

1. Introduction

Iron-containing mesoporous materials have received considerable attention because of their activity as catalyst in various acidic or oxidation reactions [1–3]. We have recently shown that iron-containing mesoporous silica is an efficient catalyst in the alkylation of benzene with benzyl chloride and that this efficiency is related to the redox properties of iron in a mechanism involving a redox step at the reaction initiation [4]. The alkylation agent is oxidized with formation of a charge transfer complex reacting with the aromatic molecule. In contrast to usual Lewis acids, this type of catalyst shows low sensitivity to water, can be easily regenerated, and is rather independent of the effect of substituents. Thus, it can be used with substrates of low reactivity. Furthermore, using a support with large pores does not limit the size of the reacting molecules, rendering these catalysts very attractive.

Several studies have been published on the characterization of iron-containing mesoporous silica that often show discrepancies [5–10]. The concomitant formation in the pores of several iron species, ranging from more or less isolated cations to Fe_2O_3 particles, can explain these discrepancies. The present study has been undertaken to clarify the nature of the active species in the iron-containing mesoporous silica catalysts used in the benzene benzylation reaction [4]. For that purpose, the characterization of catalysts with various iron loadings has been undertaken using X-ray diffraction, high-resolution transmission electron microscopy (HRTEM) with EDX analyses, electron spin resonance (ESR), and Mössbauer spectroscopy. In a recent publication, we demonstrated the interest of recording Mössbauer spectra between 0.055 and 4.2 K and under applied magnetic fields at 4.2 K to characterize iron oxide nanoparticles [10]. Here we report the characterization of the catalyst samples using the above-described techniques.

* Corresponding author.
E-mail address: millet@catalyse.cnrs.fr (J.M.M. Millet).

0021-9517/$ – see front matter
doi:10.1016/j.jcat.2007.03.028

2. Experimental

2.1. Synthesis of the catalysts

The Fe-hexagonal mesoporous solid (HMS) catalysts were prepared as described previously [4]. Hexadecyl-trimethylammoniumbromide (HDAB), iron nitrate ($Fe(NO_3)_3{\cdot}9H_2O$), and then tetraethylorthosilicate (TEOS) were added to water and ethanol (EtOH) solutions. The dissolution of each component was carried out until completion before the next one was added. After mixing, the resulting solutions with composition SiO_2–$(1/2n)$ Fe_2O_3–0.3 HDAB–7 EtOH–35 H_2O, where $n = 100$, 55, 50, 44, 30, 15, were stirred at room temperature for 24 h. The solids thus obtained were recovered by filtration, washed with distilled water, and air-dried at 393 K [11]. Organic molecules occluded in the mesopores were removed by dispersing the solid (5 g/100 ml) in a solution of ethanol containing NH_4Cl (1 g/100 ml) and maintained under vigorous stirring for 2 h [12]. The procedure was repeated twice before drying at 393 K and calcination at 823 K in air for 6 h. The samples are referred to as Fe-HMS-n, where n is the Si/Fe ratio in the solutions. Because the iron content of the Fe-HMS-55 solid was too low to allow the recording of Mössbauer spectra in suitable conditions, the compound was synthesized using Fe nitrate enriched with ^{57}Fe.

2.2. Characterization techniques

The chemical compositions of the samples were determined by atomic absorption. The surface areas were determined using the BET method. X-ray diffraction (XRD) patterns obtained using a Siemens D500 diffractometer and Cu$K\alpha$ radiation, were recorded with 0.02° (2θ) steps and 1 s counting time per step between 1 and 10° (2θ) and between 10 and 80° (2θ). ESR spectra were recorded in the X band mode on a Varian E9 spectrometer at 77 and 295 K. The ESR data were fed directly into a PC for processing.

Quantitative analyses of the relative populations of the identified Fe species were performed. Spectra of several solids were recorded after treatment overnight under vacuum at 445 K. DPPH (3314 G, $g = 2.0036$) was used as a standard for g-value determinations.

High-resolution transmission electron micrography (HRTEM) and electron diffractography were done using a JEOL 2010 equipment operating at 200 kV with a high-resolution pole piece and an energy-dispersive X-ray spectrometer (EDX; Link Isis, Oxford Instruments). The samples were either dispersed in ethanol using a sonicator. A drop of the suspension was dripped onto a carbon film supported on a copper grid, and ethanol was quickly evaporated or included in an EPON resin to prepare thin slices (20–40 nm) by ultramicrotomy. The slices were recovered on a microscopic copper grid (3.05 mm; 200 mesh) coated with a holey-carbon film. EDX studies were carried out using a 15-nm probe to analyze the smallest particles. Standard deviations were evaluated for atomic ratio from at least 10 analyses.

Table 1
Chemical analysis and BET surface area measurements data

Sample	Chemical analysis		Surface area (m^2/g)
	Fe (wt%)	Si/Fe	
HSM	0.00	–	1170
Fe-HMS-100	0.75	80.0	1162
Fe-HMS-50	1.66	54.6	1135
Fe-HMS-44	2.12	42.5	1106
Fe-HMS-30	3.70	23.8	935
Fe-HMS-15	6.08	14.0	698

The ^{57}Fe Mössbauer spectra of the samples were recorded between 298 and 4.2 K using a 2-GBq ^{57}Co/Rh source and a conventional constant acceleration spectrometer, operated in triangular mode. Spectra at temperatures below 4.2 K were obtained in a ^{3}He–^{4}He dilution refrigerator and in-field spectra with a superconducting coil. The applied magnetic field (H) was parallel to the γ-ray direction of propagation. The isomer shifts (δ) are given with respect to α-Fe at 293 K and calculated as the quadrupolar splittings (Δ) with a precision of about 0.02 mm/s. The validity of the computed fits was evaluated on the basis of both χ^2 values and convergence of the fitting process. The relative areas of the observed components were used to quantitatively evaluate the relative amounts of the iron species present in the catalysts, assuming equal recoil-free fractions for all catalysts.

3. Results

3.1. XRD, BET surface area, and chemical analysis

The Si/Fe ratio of the compounds was varied over a very wide range (15100) to characterize all of the iron species that may be formed in this type of compound. The elemental analyses of the synthesized compounds, presented in Table 1 with their BET surface areas, correspond well to the nominal values. All of the surface areas are 1100–1200 m^2/g except those of the two compounds with the highest iron loading, which are lower.

The XRD patterns of the compounds have been reported previously [4]. They are typical of mesoporous-type silica material, not well crystallized, with a broad peak at $d = 3.2$ nm. The intensity of this peak decreases with increasing iron content, demonstrating that adding iron has a negative effect on crystallinity. At the same time, small peaks corresponding to α-Fe_2O_3 (hematite form) appear and increase with increasing iron content. The UV spectra of the samples Fe-HMS-100, -50, and -15 have been reported previously [4]. The spectrum of the Fe-HMS-100 catalyst shows two absorption bands at 230 and 245 nm, corresponding to oxygen-to-metal charge transfers involving isolated tetrahedrally coordinated ferric cations. When the iron content of the solids increases, a very broad band appears with a maximum around 350 nm [4]. The presence of this band, which is characteristic of iron oxide, is in good agreement with the XRD data.

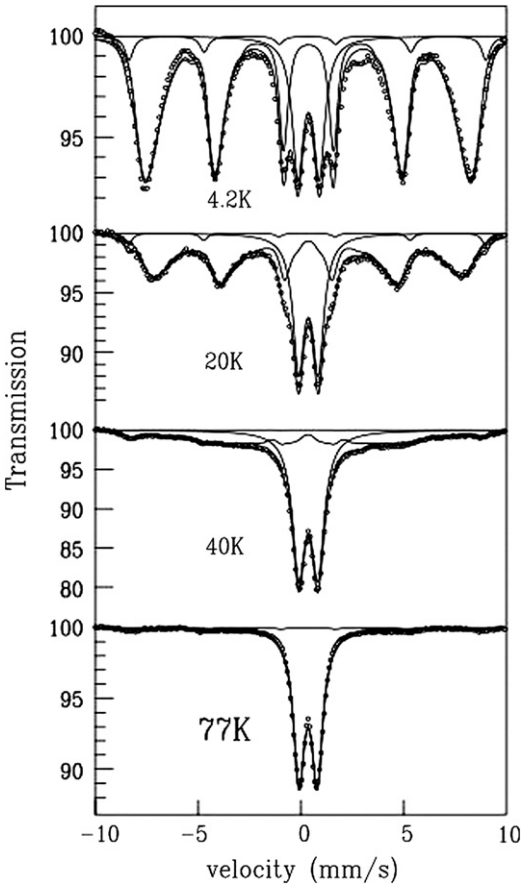

Fig. 1. ^{57}Fe Mössbauer absorption spectra of the Fe-HMS-55 catalyst at different temperatures between 77 and 4.2 K.

3.2. ^{57}Fe Mössbauer spectroscopy

The spectra of the as-prepared compounds recorded at 295 K show the same ferric doublet, with an isomer shift $\delta = 0.33 \pm 0.02$ mm/s and a quadrupolar splitting $\Delta = 0.86 \pm 0.02$ mm/s. Along with the doublet, the richer iron catalyst (Fe-HMS-15) exhibits a magnetic sextet (relative intensity 81%). This sextet, with a quadrupolar splitting of $\Delta = -0.22$ mm/s and a hyperfine field of 52.0 T, can be assigned without ambiguity to hematite α-Fe_2O_3 [13]; this correlates well with the XRD analysis of the sample showing the presence of such a phase.

To evaluate the doublet observed at room temperature, we recorder spectra at lower temperatures. The spectra obtained for Fe-HMS-55 at temperatures between 77 and 4.2 K are presented in Fig. 1. Like in the other samples (Fe-HMS-35 and Fe-HMS-50), they initially show two components: a quadrupolar doublet, visible even at 4.2 K, and a magnetic sextet with rather broad lines. However, at intermediate temperatures [i.e., 30 K (see Fig. 1) and 40 K], another weak intensity (5%) magnetic sextet is visible, with a large hyperfine field (H_{hf}) of 54 T and rather narrow lines. At 77 K, only this sextet is present with a quadrupolar doublet. The isomer shifts of these components are similar: $\delta = 0.47$ mm/s, typical for ferric compounds at low temperature. At this stage, we can identify two Fe species in the spectra: hematite (α-Fe_2O_3), corresponding to the 5% sextet with $H_{hf} = 54$ T, and a superparamagnetic

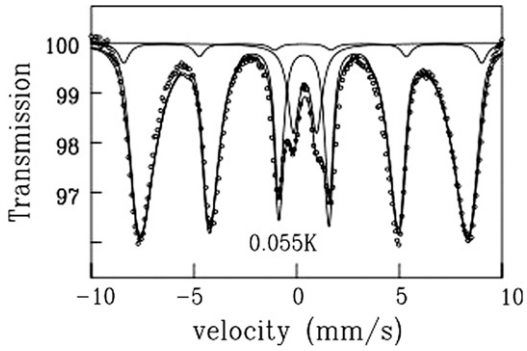

Fig. 2. ^{57}Fe Mössbauer absorption spectrum of the Fe-HMS-55 catalyst at 0.055 K.

oxide-like species [14], giving rise to the doublet and main sextet. As temperature increases, the growing of the intensity of the doublet at the expense of the sextet is a behavioral characteristic of nanosized magnetic particles, due to the increasing number of particles with rapidly fluctuating magnetization, that is, with a time scale shorter than the hyperfine Larmor time $\tau_L \cong 10^{-8}$ s associated with ^{57}Fe [15]. The magnetization (or Néel vector) of a particle with volume V fluctuates according to an Arrhenius law, $1/\tau = 1/\tau_0 \exp(-U/k_B T)$, where $\tau_0 \cong 10^{-10}$–10^{-11} s is a microscopic trial time and $U = KV$ is the anisotropy barrier, K being the density of anisotropy energy ($K \cong 10^4$–10^5 ergs/cm^3) characteristic of the material. The "blocking volume" $V_b(T)$ at temperature T for ^{57}Fe Mössbauer spectroscopy is such that $1/\tau = 1/\tau_L$; it is given by the expression $V_b(T) = k_B T/K \cdot \ln(\tau_L/\tau_0)$, and it is an increasing function of T. Thus, as temperature increases, more and more particles have $V < V_b$, implying $1/\tau > 1/\tau_L$, and show a spectrum in which the magnetic hyperfine interaction has been smeared out, leaving the quadrupolar doublet alone. In Fig. 1, the magnetic hyperfine sextet with broad lines has been accounted for by a distribution (histogram) of hyperfine fields with a peak value decreasing from 50 T at 4.2 K to around 35 T at 40 K. The splitting of the quadrupolar doublet is $\Delta = 0.94(2)$ mm/s in this low-temperature range.

To check whether a quadrupolar doublet is still present below 4.2 K, a study of the Fe-HMS-55 sample was conducted at low temperature. Spectra were recorded at 1 K and 0.055 K (Fig. 2). At 0.055 K, a sizeable quadrupolar doublet (11%) is seen, but with hyperfine parameters [$\delta = 0.53(2)$ mm/s and $\Delta = 1.15(3)$ mm/s], slightly different than those of the superparamagnetic doublet observed at higher temperature. The persistence of a doublet down to temperatures as low as 0.05 K already has been observed for several iron oxide-supported catalysts [10,16]. For small magnetic particles, fluctuations of magnetization are "frozen" below 1 K with respect to the Larmor time τ_L. Thus, the presence of the doublet demonstrates rapid magnetic relaxation at very low temperature and can be related either to "isolated" ferric iron, for which only long-range dipolar interaction exists, or to ferric cations forming small oligomers (e.g., dimers, trimers), also allowing rapid exchange-driven spin fluctuations.

Therefore, the Fe-HMS-55 sample has the following composition (in Fe at%): 11% in small oligomers, 4% in hematite,

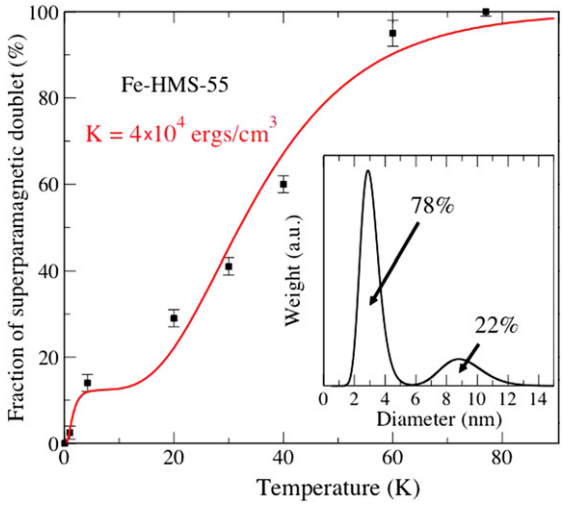

Fig. 3. Variation of the fraction of the superparamagnetic doublet intensity as a function of temperature in the Fe-HMS-55 compound. The solid line is a calculation using the particle size distribution shown in the inset and a value of the anisotropy constant $K = 4 \times 10^4$ ergs/cm^3.

and 85% in an oxide-like superparamagnetic species. To further characterize this latter species, Fig. 3 plots the thermal variation of the fraction of its quadrupolar doublet. It rises rapidly up to 4 K, then more slowly, with an S-like shape, up to 80 K, at which point it reaches 100%. This two-stage evolution points to the existence of a bimodal size distribution for the superparamagnetic particles. The inset in Fig. 3 shows the size distribution (modeled as two normalized lognormal functions) required to reproduce the experimental thermal variation of the doublet fraction, assuming a density of anisotropy energy of $K = 4 \times 10^4$ erg/cm^3. The superparamagnetic fraction is calculated as

$$f_p(T) = \frac{1}{\langle V \rangle} \int_{V_{min}}^{V_b} V f(V)\, dV,$$

where $f(V)$ is the size distribution function. The solid line in Fig. 3 is the calculated curve; above about 5 K, all of the smaller particles [mean diameter 3 nm (78% in number, but 12% in volume)] are superparamagnetic, and the larger particles (mean diameter 9 nm) reach the superparamagnetic regime at 80 K. This bimodal size distribution qualitatively corresponds to that shown in the HRTEM images (see Section 3.4), demonstrating the larger particles correspond to agglomerations of the smaller particles.

To obtain clues about the magnetic structure of the observed Fe species, spectra were recorded in the Fe-HMS-55 sample at 4.2 K with applied magnetic fields of 2 and 7 T (Fig. 4). The recorded spectra show components similar to those distinguished at 4.2 K in zero field: antiferromagnetic hematite, a doublet-like subspectrum, and a broad sextet. As the applied field increases, the intensity of the intermediate lines of the sextet strongly decreases. This shows that the hyperfine fields of the Fe^{III} species progressively reorient toward the field. At the same time, the hyperfine field distribution center decreases from 50 T in zero field to 46 T at 7 T. This type of response to the

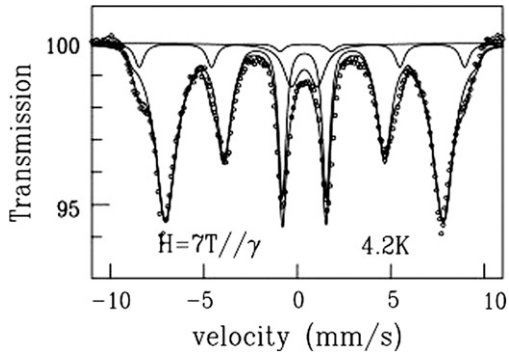

Fig. 4. ^{57}Fe Mössbauer absorption spectrum of the Fe-HMS-55 catalyst at 4.2 K with a magnetic field of 7 T applied parallel to the γ-ray direction of propagation.

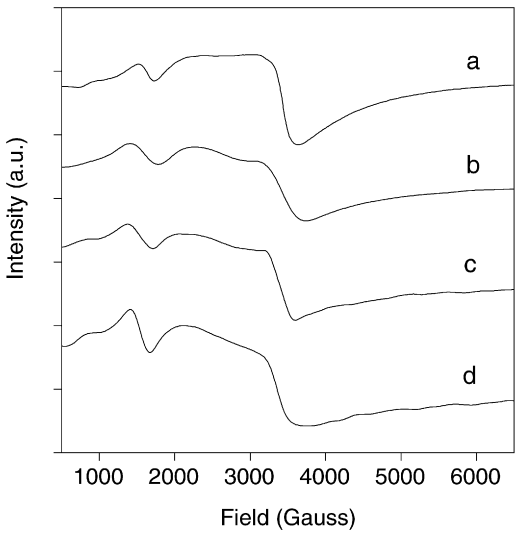

Fig. 5. ESR spectra of the compounds recorded at 77 K: (a) Fe-HMS-15, (b) Fe-HMS-30, (c) Fe-HMS-50, (d) Fe-HMS-100.

field is typical of a ferromagnetic ordering; for Fe^{III}, the hyperfine field is antiparallel to the magnetic moment, which aligns along the applied field. The same behavior has already been observed for iron oxide supported on zirconia and attributed to Fe^{III} clusters or "rafts" in solid solution within the first surface layer of the solid.

3.3. ESR spectroscopy

EPR spectra of the compounds were recorded at 77 K under N_2 (Fig. 5) and after dehydration under vacuum at 623 K (Fig. 6). The integrated intensity of the total spectra appears to be proportional to the Fe content of the samples except for the Fe-HMS-15, which exhibits large antiferromagnetic hematite particles identified by XRD and Mössbauer spectroscopy (Fig. 7). Four signals at $g = 7.4$, 4.3, 2.3, and 2.0 can be distinguished. The signal at $g = 4.3$ is currently observed for iron oxide catalysts supported on various substrates and attributed to isolated octahedral or tetrahedral Fe^{III} sites with a strong rhombic distortion [17,18]. The smallest and broader signal at $g = 7.4$ was previously observed in the same type of solids but not assigned [19]. The signal at $g = 2$ often has

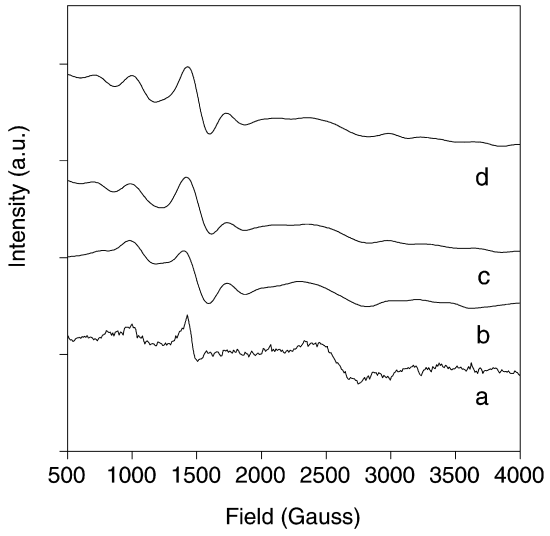

Fig. 6. ESR spectra of the compounds recorded at 77 K after reduction at 623 K under vacuum: (a) Fe-HMS-15, (b) Fe-HMS-30, (c) Fe-HMS-50, (d) Fe-HMS-100.

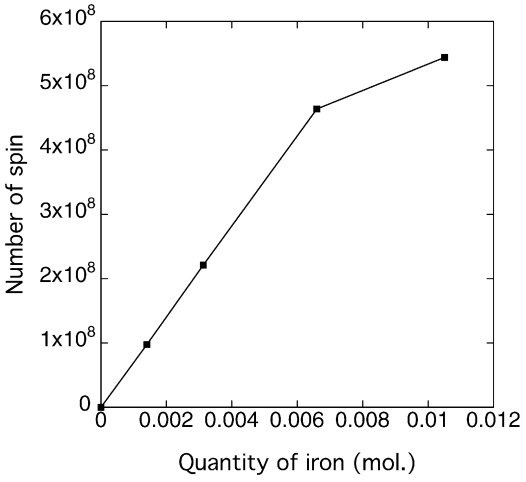

Fig. 7. Variation of the total intensity of the ESR spectra as a function of the iron loading of the compounds.

been attributed to octahedrally coordinated Fe^{III} cations; it has been proposed to generally correspond to extra-framework iron species observed in zeolitic material characterization and can be assigned to the superparamagnetic iron oxide clusters [20–22]. The interpretation of the small signal at $g = 2.3$, which also is frequently detected in iron-supported catalysts or zeolites, is still matter of debate. It has been assigned either to small iron oxide aggregates or to 3-coordinated species in the framework of zeolitic materials [23]. The latter species is sensitive to adsorbed molecules like H_2O. When attributed to small aggregates, it generally disappears after heat treatment under a reducing atmosphere or vacuum because of the reduction of iron, whereas it increases when attributed to the second species due to desorption of adsorbed molecules. In the present study, the signal, which is very small, apparently increased after heat treatment under vacuum and may be attributed to 3-coordinated species, although a partial attribution to iron oxide aggregates cannot be excluded in view of the other characterization data. Three-coordinated species are formed by either dehydroxylation or dehydration of 4-coordinated hydroxylated species.

After dehydration under vacuum at 623 K, the main signal at $g = 2$ disappeared, whereas those at $g = 4.3$ and 2.3 were still present. The disappearance of the first signal may be related to the reduction of the very small "nanoparticles." Such reduction did not seem to affect the other species, which may be attributed to oligomeric iron species in more or less solid solution in the silicic mesoporous walls and corresponding to those giving a doublet in the Mössbauer spectra even at very low temperature (0.055 K). A new signal characterized by a $g = 6.1$ appears. Such a signal was previously observed with two other signals with $g = 4.3$–9 for FeS-1 outgassed at 673 K [24]. It was assigned to a distorted tetrahedron, which maintains an axial C_{3v} asymmetry. Finally, we observed that the transformation was totally reversible; treating the material for 24 h at room temperature in ambient air restored the original spectrum.

3.4. HRTEM with EDX analyses

We studied the morphology of the Fe species within the mesoporous material by HRTEM on the compound Fe-HMS-50 (Figs. 8a and 8b). Two types of dark-phase contrast attributed to iron oxide from EDX analyses were observed: one type corresponding to spherical spots of large size (>50 nm in diameter) and another type corresponding to thin oxide layers forming 10–30 nm "rafts." It is interesting to note that such spherical and elongated morphologies were previously reported for the same type of materials [7]. The large particles, as could be predicted, lie only at the surface of the mesoporous material, whereas the oxide layer is present both at the surface and in the mesopores of the material; in the latter case, a decrease in concentration from the border to the center of the particles was observed. Besides these two main species, it has been possible to detect very small spherical darker spots either isolated from the silica or dispersed in the oxide layer. Contrast profiles were recorded over these spots to evaluate the spot size, which are around 1–2 nm (Fig. 9). These spots correspond to very small iron oxide particles completely isolated or present in the iron oxide "rafts," which should simply correspond to the agglomeration of these small particles. The fact that only some of the particles appear darker in the "rafts" could be related to their orientation in Bragg position with respect to the electron beam.

4. Discussion

The characterization results obtained from XRD, Mössbauer, and ESR spectroscopies and from HRTEM images evidence the presence of Fe species in different forms at the surface or in the mesoporous silica. The first type of species corresponds to isolated species or to very small oligomers (e.g., dimers, trimers) with iron cations close enough to each other to interact and lead to exchange fluctuations but not large enough to allow magnetic ordering. This type, accounting for about 10% of the Fe^{III} ions, yields, in Mössbauer spectra, a paramagnetic doublet down to the lowest temperature (0.05 K) and in

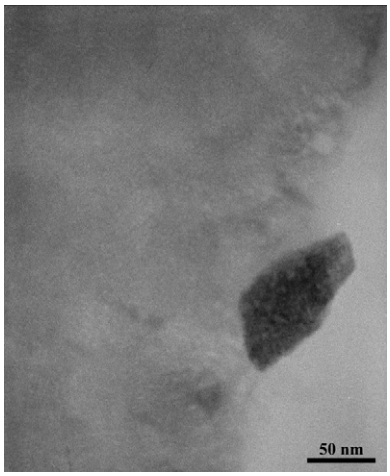

(a)

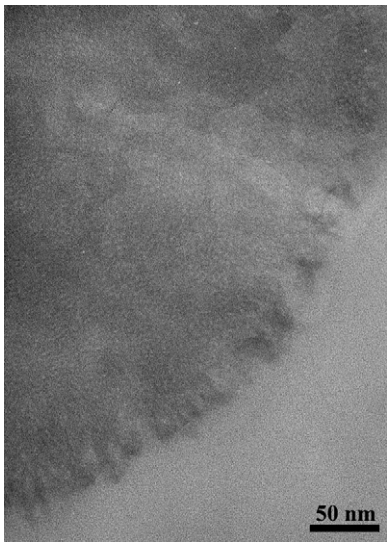

(b)

Fig. 8. High-resolution transmission electron imaging of a slice of the Fe-HMS-50 compound showing a large iron oxide particles at the surface of the grains (a) and agglomeration of smaller particles (b).

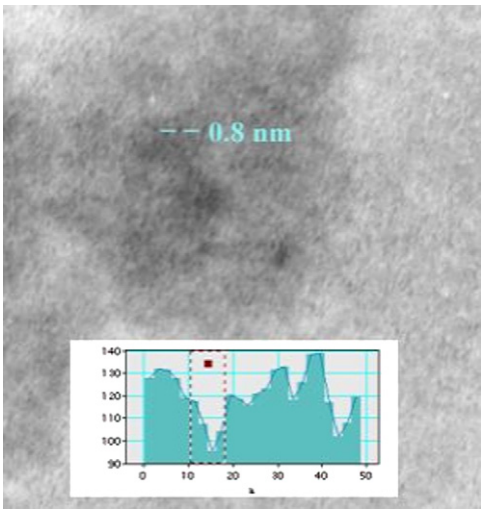

Fig. 9. High-resolution transmission electron imaging of the Fe-HMS-50 compound showing the agglomerated very small particles with a profile of grey level histogram along the line and across a particle in Bragg position. Support grey level defined the baseline.

ESR spectra to signals with g values varying with the symmetry or coordination of the Fe^{III} cations but different from 2.0. It is noteworthy that the relative intensity of the latter signals is of the same order as in the Mössbauer spectra.

The second species corresponds to larger iron oxide oligomers undergoing magnetic ordering and forming superparamagnetic nanoparticles. These nanoparticles have an approximate diameter of 1–3 nm, small enough so that the fluctuation frequency of the magnetization is faster than 10^8 s^{-1} at 4.2 K (12% of the Fe^{III} cations). Their narrow size distribution originates from the fact that they should have been formed in the silica mesopores during the preparation heat treatment. As shown by electron microscopy, these particles tend to agglomerate, forming large "rafts" at the surface of the silica walls, and to exit from the mesopores to reach the surface of the silica particles. These agglomerations of nanoparticles, which account for approximately 72% of the Fe^{III} cations, behave as larger particles from a magnetic standpoint. They show a decrease in the relaxation time (i.e., increased blocking temperature) because of the magnetic interaction with each other. The correlation that arises between magnetization vectors of neighboring particles is the main cause of the decreased relaxation time. The influence of the magnetic interactions due to particle agglomeration on the superparamagnetic relaxation has been reported previously [25–27], and models based on dipolar interactions have been developed [25,28]. The third species (5%) consists of hematite particles identified by XRD and Mössbauer spectroscopy. The decreased surface area of the samples with increasing iron content could be related to the formation of these particles.

A peculiar feature of the very small particles isolated or forming "rafts" is the ferromagnetic nature of their magnetic ordering, which differentiates them from the larger bulky particles, which are antiferromagnetic (hematite). This is clearly demonstrated by the Mössbauer spectra recorded with an applied magnetic field at 4.2 K. Recent studies have reported that the surface of a magnetic material generally has magnetism different than that of the bulk, because the translational symmetry is broken at the surface. For the same reason, nanometric iron oxide particles may exhibit an unusual ferromagnetism. In that respect, ferromagnetic order at the surface of a paramagnetic FeO(111) film formed on a Fe(110) crystal has been reported [29]. When the number of Fe^{III} ions interacting magnetically in a cluster is sufficiently large to allow collective effects to emerge, the paramagnetic resonance changes to a ferromagnetic resonance response. The resonance intensity is proportional to the susceptibility, which is much higher in the ferromagnet because of the high spontaneous magnetization [30].

When the iron content of the sample increases, the relative amount of hematite and the size of the agglomerated "rafts" increase (equivalent particle diameter of 15–20 nm for Fe-HMS-30). In the same way, the Fe-HMS-100 is likely to contain mainly oligomeric species. In terms of the benzene benzylation reaction for which the present catalysts have been tested, the proposed mechanism involves oxidation of benzyl chloride on iron cations with formation of a charge transfer complex [4],

$$\Phi\text{-}CH_2Cl + Fe^{3+} \rightarrow \Phi\text{-}CH_2^{\cdot+} + Cl^{\cdot},$$

$$\Phi\text{-}CH_2^{\cdot+} \rightarrow \Phi\text{-}CH_2^{+} + Fe^{2+},$$

$$Fe^{2+} + Cl^{\cdot} \rightarrow Fe^{3+} + Cl^{-},$$

$$\Phi\text{-}CH_2^{+} + ArH \rightarrow \Phi\text{-}CH_2\text{–}Ar + H^{+}.$$

Apparently, whereas Fe-HMS-55, -50, and -30 have increasing but comparable activity, the Fe-HMS-100 sample is completely inactive [4]. Although this feature is not completely understood, the iron cations possibly may be much less reducible in the catalytic reaction conditions when in the form of small oligomeric or almost isolated species in strong interaction with the support rather than in oxide nanoparticles. On the other hand, the latter should reduce much more easily than larger particles. The high oxidation state of iron in bulk oxide is stabilized by the Madelung potential, whereas this is not the case for very small oxide particles. In that respect, a similar trend was observed in the case of Fe-hydrotalcite in the reduction of nitro aromatic compounds by hydrazine hydrate [31] and of Fe-sulfated zirconia used in *n*-butane isomerization [16].

5. Conclusion

The characterization by XRD, ESR, and Mössbauer spectroscopy of Fe-HMS materials, which are active and selective catalysts for the alkylation of benzene with benzyl chloride reaction, has shown that several iron species could be identified at the surface of the pore walls of the mesoporous silica, including (i) very small Fe^{III} oligomers or isolated cations close to each other, remaining paramagnetic down to very low temperature (0.05 K); (ii) superparamagnetic nanometric or subnanometric small clusters undergoing a ferromagnetic type of ordering; and (iii) antiferromagnetic large hematite particles. In the catalysts with an Si/Fe ratio of around 50, iron is present mainly as nanometric clusters. With increasing iron content (Si/Fe = 15), the large hematite particle content increases, whereas with decreasing iron content (Si/Fe = 100), the oligomer content is maximized. The absent reactivity of the catalysts with low iron content hypothetically may be attributed to the fact that iron cations that are almost isolated or in very small oligomers cannot be reduced under the reaction conditions.

Finally, our findings clearly demonstrate the great interest of recording Mössbauer spectra below 4.2 K. This provided evidence of the formation of nanometric iron clusters at the surface of the mesoporous silica. Standard low-temperature studies, as have been conducted in the vast majority of cases above 4.2 K, would have concluded to the presence of larger particles; the analysis by Mössbauer spectroscopy performed at lower temperature demonstrated that these particles were agglomerations of nanometric iron clusters. The spectroscopic technique performed below 4.2 K allowed us to reach another level of resolution of the ferric particle structures.

References

[1] A. Corma, Chem. Rev. 97 (1997) 2373.
[2] X.S. Zhao, G.Q. Lu, G.J. Millar, Ind. Eng. Chem. Res. 35 (1996) 2075.
[3] P. Decyk, M. Trejda, M. Ziolek, C. R. Chim. 8 (2005) 635.
[4] K. Bachari, J.M.M. Millet, B. Benaïchouba, O. Cherifi, F. Figueras, J. Catal. 221 (2004) 55.
[5] A.B. Bourlinos, M.A. Karakassides, D. Petridis, J. Phys. Chem. B 104 (2000) 4375.
[6] A.B. Bourlinos, A. Simopoulos, N. Boukos, D. Petridis, J. Phys. Chem. B 105 (2001) 7432.
[7] L. Zhang, G.C. Papaefthymiou, J.Y. Ying, J. Phys. Chem. B 105 (2001) 7414.
[8] R. Köhn, D. Paneva, M. Dimitrov, T. Tsoncheva, I. Mitov, C. Minchev, M. Fröba, Microporous Mesoporous Mater. 63 (2003) 125.
[9] P.B. Amama, S.L. Dragos, C.Y. Yang, L. Pfefferle, G.L. Haller, J. Phys. Chem. B 109 (2005) 2645.
[10] J.M.M. Millet, H. Knözinger, P. Bonville, J. Phys. Chem. B 110 (2006) 16003.
[11] A. Tuel, I. Arcon, J.M.M. Millet, J. Chem. Soc. Faraday Trans. 94 (1998) 3501.
[12] B. Echchahed, B.A. Moen, L. Nicolson, L. Bonneviot, Chem. Mater. 9 (1997) 1716.
[13] O.C. Kistner, A.W. Sunyar, Phys. Rev. Lett. 4 (1960) 412.
[14] L. Néel, Ann. Geophys. 5 (1949) 99;
C.P. Bean, J.D. Livingstone, J. Appl. Phys. 30 (1959) 120S.
[15] S. Mørup, J.A. Dumesic, H. Topsøe, in: R.L. Cohen (Ed.), Applications of Mössbauer Spectroscopy, vol. II, Academic Press, New York, 1980.
[16] J.M.M. Millet, M. Signoretto, P. Bonville, Catal. Lett. 64 (2000) 135.
[17] R. Aasa, J. Chem. Phys. 52 (1983) 3919.
[18] D. Golfarb, M. Bernardo, K.G. Strohmaier, D.E.W. Vaughan, H. Thomann, J. Am. Chem. Soc. 116 (1994) 6344.
[19] P. Selvam, S.E. Dapurkar, S.K. Badamali, M. Murugasan, H. Kuwano, Catal. Today 68 (2001) 69.
[20] K. Arata, I. Oyoshima, Chem. Lett. 929 (1974).
[21] K. Arata, K. Yabe, I. Oyoshima, J. Catal. 44 (1976) 385.
[22] X. Carrier, P. Lukinskas, S. Kuba, L. Stievano, F. Wagner, M. Che, H. Knözinger, Chem. Phys. Chem. 5 (2004) 1191.
[23] D.H. Lin, G. Coudurier, J.C. Vedrine, Stud. Surf. Sci. Catal. 49 (1989) 1431.
[24] S. Bordiga, R. Buzzoni, F. Geobaldo, C. Lamberti, E. Giamello, A. Zecchnina, G. Leofanti, G. Petrini, G. Tozzola, G. Vlaic, J. Catal. 158 (1996) 486.
[25] J.L. Dormann, R. Cherkaoui, L. Spinu, M. Nogues, F. Lucari, F. D'Orazio, D. Fiorani, A. Garcia, E. Tronc, J.P. Jolivet, J. Magn. Magn. Mater. 187 (1998) L139.
[26] M.F. Hansen, S. Morup, J. Magn. Magn. Mater. 184 (1998) 262.
[27] M.A. Polikarpov, I.V. Trushin, S.S. Yakimov, J. Magn. Magn. Mater. 116 (1992) 372.
[28] S. Morup, E. Tronc, Phys. Rev. Lett. 72 (1994) 3278.
[29] Koike, T. Furukawa, Phys. Rev. Lett. 77 (1996) 3921.
[30] F. Schmidt, T. Meeder, Surf. Sci. 106 (1981) 397.
[31] J. Sanchez-Valente, J.M.M. Millet, L. Fournes, F. Figueras, Hyperfine Interact. 131 (2000) 43.